

The mass loss of C-rich giants ★,★★,★★★

J. Bergeat and L. Chevallier

Centre de Recherche Astronomique de Lyon (UMR 5574 du CNRS), Observatoire de Lyon,
9 avenue Charles André, 69561 St-Genis-Laval cedex, France

Received 12 May 2004 / Accepted 23 July 2004

Abstract. The mass loss rates, expansion velocities and dust-to-gas density ratios from millimetric observations of 119 carbon-rich giants are compared, as functions of stellar parameters, to the predictions of recent hydrodynamical models. Distances and luminosities previously estimated from HIPPARCOS data, masses from pulsations and C/O abundance ratios from spectroscopy, and effective temperatures from a new homogeneous scale, are used. Predicted and observed mass loss rates agree fairly well, as functions of effective temperature. The signature of the mass range $M \leq 4 M_{\odot}$ of most carbon-rich AGB stars is seen as a flat portion in the diagram of mass loss rate vs. effective temperature. It is flanked by two regions of mass loss rates increasing with decreasing effective temperature at nearly constant stellar mass. Four stars with detached shells, i.e. episodic strong mass loss, and five cool infrared carbon-rich stars with optically-thick dust shells, have mass loss rates much larger than predicted values. The latter (including CW Leo) could be stars of smaller masses ($M \approx 1.5 - 2.5 M_{\odot}$) while $M \approx 4 M_{\odot}$ is indicated for most of the coolest objects. Among the carbon stars with detached shells, R Scl returned to a predicted level (16 times lower) according to recent measurements of the central source. The observed expansion velocities are in agreement with the predicted velocities at infinity in a diagram of velocities vs. effective temperature, provided the carbon to oxygen abundance ratio is $1 \leq \epsilon_C/\epsilon_O \leq 2$, i.e. the range deduced from spectra and model atmospheres of those cool variables. Five stars with detached shells display expansion velocities about twice that predicted at their effective temperature. Miras and non-Miras do populate the same locus in both diagrams at the present accuracy. The predicted dust-to-gas density ratios are however about 2.2 times smaller than the values estimated from observations. Recent drift models can contribute to minimize the discrepancy since they include more dust. Simple approximate formulae are proposed.

Key words. stars: AGB and post-AGB – stars: carbon – stars: mass loss

1. Introduction

The observations of CO and HCN lines in the millimetric range together with infrared fluxes, especially from the IRAS catalogue (1988), provide estimates of parameters of the circumstellar envelopes of carbon-rich giants. They are essentially TP-AGB stars, i.e. late stages of stellar evolution of low and intermediate mass stars, experiencing substantial mass loss. This latter phenomenon may terminate their evolution on the AGB before rapid nucleosynthesis forces them to leave that branch. Mass loss also contributes to the replenishment of the interstellar medium in carbonaceous material (dust and gas), mostly from extreme (“infrared”) carbon stars. Models and simplifying assumptions are required to derive the estimates of the mass loss rate \dot{M} in solar mass per year, the expansion velocity v_e in kilometer per second, and the dust-to-gas mass density ra-

tio. For instance a model for the photodissociation of the circumstellar CO by Mamon et al. (1988) is usually applied to radial brightness distributions with fair success, but clear deviations were noted in a few cases (e.g. Schöier & Olofsson 2001). Predominant species, like hydrogen or helium, are not traced out and the adopted abundances influence the estimates of the total mass loss rate. The estimated distances are also of paramount importance since the rate calculated from observations increases as the squared distance. A full discussion is outside the scope of the present paper and we refer the reader to the papers cited in Sect. 2.

It has become clear that the interaction of pulsation and dust formation plays a key role in the mass loss phenomenon (e.g. Wallerstein & Knapp 1998 for a review). The effects of stellar pulsation are simulated in dynamical models by applying a piston at the inner boundary. Consistent models of circumstellar dust shells around carbon-rich long period variables (LPV) include time-dependent hydrodynamics, a detailed treatment of the processes of formation, growth and evaporation of dust grains, a carbon-rich chemistry, and radiative transfer (e.g. Fleischer et al. 1992, Fleischer 1994, Winters et al. 1994b, 1995, Höfner et al. 1995, 1996). The empirical Reimers relation for RGB (Reimers 1975) proved its inadequacy for AGB.

Send offprint requests to: J. Bergeat

* This research has made use of the Simbad database operated at CDS

** Partially based on data from the ESA HIPPARCOS astrometry satellite

*** Table 3 is only available in electronic form at the CDS via anonymous ftp 130.79.128.5

Table 1. Mean distances (pc) of carbon-rich giants and dispersions as obtained from data of various authors: O93 stands for Olofsson et al. (1993a), G99 for Groenewegen et al. (1999), SO1 for Schöier & Olofsson (2001), GO2 for Groenewegen et al. (2002b), and L93 for Loup et al. (1993). They are compared with astrometric data from Bergeat et al. (2002a, 2002b=BKR) for (n) stars in common. Ratios to BKR means are then quoted in the last line (See text for a discussion).

n	O93	BKR	n	G99	BKR	n	O93	SO1	BKR	n	GO2	BKR	n	L93	BKR
104	707	708	11	1141	1161	54	567	427	614	25	1535	748	21	721	536
	± 218	± 258		± 459	± 452		± 171	± 166	± 218		± 927	± 357		± 424	± 182
	1.00			0.98			0.92	0.70			2.05			1.35	

Alternative relations were derived from observational results and/or theoretical models of mass loss (e.g. Volk & Kwok 1988, Vassiliadis & Wood 1993, Blöcker 1995). The mass loss relation of Dominik et al. (1990) was the first one based on detailed calculations of dust formation and growth (Gail & Sedlmayr 1988), with rather extreme stellar parameters adapted to the very late stages of AGB evolution. Approximate formulae for mass loss rate, expansion velocity and dust to gas density ratio were then calculated by Arndt et al. (1997). They considered six stellar parameters as independent ones, namely the temperature, the luminosity, the mass, the abundance ratio of carbon to oxygen, the pulsational period and the velocity amplitude of the pulsation. They then derived approximate equations on the basis of 48 dynamical models, exploring various ranges for the six parameters. They also compared their results to those of 22 analogous models from Höfner & Dorfi (1997) who proved to be well approximated by their set of equations.

The predictions of Arndt et al. are compared to the data deduced from observations as published by various authors. We use the effective temperatures of Bergeat et al. (2001) as stellar temperatures. Using a new homogeneous scale constructed from model atmospheres, observed angular radii and spectral energy distributions, they have proved efficient in solving various problems. We also adopt the distances and luminosities derived by Bergeat et al. (2002b) from the HIPPARCOS data (1997) by taking into account three distinct biases (their Sect. 2.3; see also Knapik et al. 1998 and Bergeat et al. 2002a). Pulsation masses were derived for carbon-rich LPVs by Bergeat et al. (2002c). The carbon to oxygen (C/O) ratios were taken from Lambert et al. (1986), Olofsson et al. (1993b) and Abia & Isern (1996). The periods of pulsation used are the photometric periods taken from the General Catalogue of Variable Stars (GCVS; Kholopov et al. 1985) or from the HIPPARCOS data (1997). The values are those of fundamental mode pulsators from the study of Bergeat et al. (2002c). Considering the complexities of those pulsating atmospheres and the uncertainties on transfer in their models, we adopt the reference value $\Delta u = 2 \text{ km s}^{-1}$ of Arndt et al. (1997) for the velocity amplitude of the pulsation. We shall see that its influence is quite limited.

We re-scaled the mass loss rates from the literature to the distances of Bergeat et al. (2002b) and a f-correction was applied to convert them to the scale of Schöier & Olofsson (2001) who properly dealt with radiative transfer (Sect. 2). In addition, the expansion velocities and dust-to-gas density ratios were compiled for a sample of carbon-rich giants (Sect. 2). The

available predictions from hydrodynamical models are summarized in Sect. 3 and equations fitted on a grid from the literature are adopted. Values of stellar parameters from Bergeat et al. (2001, 2002b, 2002c) were compiled for stars in common with millimetric studies and mean values collected for eight photometric groups (Sect. 4) to be replaced in the formulae of Arndt et al. (1997). Then, the comparison of observed and predicted mass loss rates is performed in a diagram against effective temperature (Sect. 5). In a similar approach, the observed and predicted expansion velocities are compared by plotting *vs.* effective temperature (Sect. 6). The discrepancy noted between observed and predicted dust-to-gas density ratios, is estimated and discussed (Sect. 7). A few conclusions are given and discussed (Sect. 8) and simple approximate formulas are proposed in Appendix A.

2. The data from millimetric observations

Mass loss rates, expansion velocities and dust-to-gas density ratios were extracted from the literature for a large sample of carbon-rich giants. The early millimetric data and results are summarized in a catalogue by Loup et al. (1993). Schöier & Olofsson (2001) revised a set of data from Olofsson et al. (1993a, 1993b). The mass loss rate, for stars in common, is on average 3.1 ± 3.6 times larger in the 2001 paper than it was in those of 1993. Values in Groenewegen et al. (2002a) for 18 stars in common with Olofsson et al. are on average 2 times larger. A mean 2.9 ratio was found from two stars in common with Winters et al. (2003). Admittedly, recent accepted values for mass loss rates are typically 2-3 times higher than the previous ones from Olofsson et al. (1993a, 1993b). We also considered data for a few stars from Groenewegen et al. (1999), Schöier & Olofsson (2000) and Le Bertre et al. (2001, 2003; see also Meixner et al. 1998 for RW LMi=CIT6 and Skinner et al. 1998 for CW Leo=IRC+10216).

Usually, the distances adopted by the authors substantially differ and this is a fundamental problem since the mass loss rate (for both gas and dust) increases as the squared distance. Large discrepancies may exist between distances estimated from various methods: mean absolute magnitude adopted, say in the K-band, mean bolometric magnitude with bolometric correction or mean luminosity, absolute magnitude *vs.* period for long period variables, kinematical methods ... The astrometric parallaxes of those bright distant giants are also affected by substantial errors. First of all, we calculated the mean distances and dispersions for the various samples of the above-mentioned references and compared them to their counterparts

Table 2. The data for 119 carbon-rich giants (Sect. 2) with variable star names (Columns 1 and 10, except for CGCS1006 in Stephenson 1989 and Alksnis et al. 2001) shown with boldface characters for 19 Miras. Data from SEDs and spectra are given: the photometric groups in Columns 2 and 11 with an additional J for ^{13}C -rich stars, the effective temperatures (Kelvin) in Columns 3 and 12, the carbon to oxygen abundance ratio (C/O) of the atmosphere in Columns 4 and 13, the absolute bolometric magnitude M_b in Columns 5 and 14, that can be translated into luminosity in solar units from Eq. (3), and the distance D_{BKR} in parsec in Columns 6 and 15. The data from millimetric observations are displayed in Columns 7 and 16 (mass loss rate as $\dot{M}' = 10^8 \dot{M}$ where \dot{M} in solar mass per year), Columns 8 and 17 (expansion or terminal velocity v_e in km s^{-1} , and Column 9 and 18 ($r' = 10^3 r$ where $r = \dot{M}_d/\dot{M}_g$ is the dust-to-gas ratio of mass loss rates). Additional notes deal with ranges: ^a HC5-CV4 & 3525-2775 K, ^b HC5-CV6 & 3520-2645 K & $M_b = -3.72; -4.36$, ^c 2290-2245 K & $M_b = -4.86; -4.53$, ^d 2920-2840 K & $M_b = -5.22; -4.80$, ^e $M_b = -5.81; -5.48$, ^f 3345-2825 K & $M_b = -6.15; -5.67$, ^g 2405-2525 K & $M_b = -5.89; -6.10$, ^h IRC+10216 1915-2105 K, ⁱ CIT6 2425-2465 K, ^j 2100-1945 K & $M_b = -5.23; -4.60$, ^k 2865-2680 K & $M_b = -5.51; -5.00$, ^l CV5-CV6 & 2650-2530 K & $M_b = -4.94; -5.06$, ^m 1885-1875 K & $M_b = -6.28; -5.93$, ⁿ 2945-2865 K & $M_b = -4.84; -5.61$, ^o 1975-1875 K, ^p 2240-2095 K & $M_b = -5.42; -5.22$, ^q CV1-CV5 & 3245-2605 K & $M_b = -3.01; -3.69$, ^r 2735-2655 K & $M_b = -4.78; -4.58$, ^s CIT 5, ^t IRAS 05352+2247, ^u AFGL 971, ^v AFGL 2067=IRC-10396, ^w AFGL 3116=IRC+40540, ^x AFGL 1235, ^y AFGL 1961 (erroneously identified as V522Oph). Not shown in Fig. 1 : according to Olofsson et al. (2000), TT Cyg (which is surrounded by a thin shell) is presently losing mass at a modest rate of $3 \cdot 10^{-8} M_{\odot} \text{ yr}^{-1}$ which is perhaps to be multiplied by the 3.9 correction factor of Eq. (2); according to Izumiura et al. (1996), Y CVn** exhibited a $7 - 20 \cdot 10^{-6} M_{\odot} \text{ yr}^{-1}$ rate at the formation of its thin shell.

Name	G	T_{eff}	C/O	M_b	D	\dot{M}'	v_e	r'	Name	G	T_{eff}	C/O	M_b	D	\dot{M}'	v_e	r'
VX And	CV6J	2520	1.76	-4.47	560	14	11.5	4.7	AQ And	CV5	2660		-5.24	1015	43		
Z Psc	CV2	3095	1.014	-4.65	465	6.1	3.5	2.9	R Scl*	CV4	2625	1.34	-5.48	475	640	16.9	0.86
R For	CV7	2000		-5.82	865	500	16.5	0.87	V623Cas	CV1J	3360		-4.49	515	11		
TW Hor	CV2	2950		-5.28	485	20	5.5	2.5	V384Per*	CV7	1820		(-5.43)	720	590	15.0	0.25
Y Per	HC5 ^a	3150 ^a		-4.09	975	29	7.2	0:	U Cam*	CV4	2695	1.30	-5.09	525	200	20.6	1.0
V466Per	CV4	2775		(-4.66)	530	24	9.0	2.3	SY Per	CV5	2705		-5.86	1430	150	17.5	0.79
ST Cam	CV4	2805	1.14	-6.07	800	110	9.0	0.89	TT Tau	CV2	3090		-4.88	585	20	5.0	0.42
V346Aur	SCV	2880		-5.49	1110	20			AU Aur	CV5	2665		-5.01	1470	57		
R Ori	HC5 ^b	3083 ^b		-3.72 ^b	1700	61	10.0	0.67	R Lep	CV6	2290 ^c	1.030	-4.86 ^c	335	160	18.0	1.4
EL Aur	CV4	2730		-4.60	650	28			W Ori	CV5	2625	1.16	-5.19	410	38	11.0	2.5
V431Ori	CV6	2540		-3.78	540	22			UV Aur	CV3	2920 ^d		-5.22 ^d	1090	160	10:	
S Aur	CV7	1940	1.014	(-5.43)	1130	420	25.5	1.0	RT Ori	CV4	2870		-4.31	675	22		
CGCS1006 ^f	CV6	2300		(-5.05)	1870	43			TU Tau	CV3	2850		-5.81 ^e	1055	57		
Y Tau	CV4	2735	1.040	-6.00	735	160	11.0	1.6	W Pic	CV6	2530		-4.85	665	51	16.0	1.7
FU Aur	CV2	3035		-5.56	1295	28			TU Gem	CV4	2715	1.12	(-4.66)	515	44	11.5	1.7
FU Mon	SCV	3085 ^f		-6.15 ^f	1450	26			V Aur	CV4	2820		-5.47	1760	360	20	0.13
BN Mon	CV6	2410		(-5.05)	1280	420	24.2	0.73	ZZ Gem	CV6	2530		(-5.05)	1835	59	6.9	0.22
BL Ori	CV2	3035	1.039	-5.13	595	25	9.0	1.2	CR Gem	CV2	2960		-5.60	920	84	14.9	1.3
UU Aur	CV4	2760	1.063	-5.78	415	76	11.0	0.16	NP Pup	CV2	3090		-4.54	510	19	9.5	1.0
RV Mon	CV3	2910		-4.90	670	17			V614Mon	CV1	3320		-3.47	485	1.5		
RY Mon	CV6	2440	1.19	-4.90	685	59	11.0	1.1	W CMa	CV3	2975	1.046	-5.42	785	61	10.5	0.63
V406Pup	CV3	2875		-4.15	610	11			RU Pup	CV3	2680		-3.33	455	13		
V346Pup ^x	CV7	1875		(-5.43)	1120	3310	20.7	0.50	R Pyc	CV6	2440		-4.52	1175	68	8.8	1.2
UZ Pyx	CV1	3325	1.30	-4.63	815	26			X Cnc	CV5	2645	1.14	-5.77	710	62	7.0	1.3
T Cnc	CV6	2405 ^g		-5.89 ^g	1085	97			CW Leo ^h	CV7	1915 ^h	1.4	-5.83	150	3300	14.5	0.66
Y Hya	CV5	2645	1.52	-4.89	485	37	9.0		X Vel	CV5	2700	1.16	-5.46	620	63	10.0	0.68
SZ Car	CV4	2810		(-4.66)	365	46	14.0	0.30	RW LMi ⁱ	CV6	2445 ⁱ		(-5.05)	410	650	17.0	4.5
XZ Vel	CV6	2430	1.22	(-5.05)	760	94	14.0	0.90	CZ Hya	CV5	2525	1.02	(-4.82)	990	125	12.0	0.65
U Ant*	CV4	2810	1.44	-4.93	320	200	21.8		U Hya	CV3	2965	1.043	-3.93	175	21	7.0	0.98
VY UMa	CV2	2930	1.060	-4.67	445	14	6.0	0.97	V Hya	CV6	2160	1.050	-5.88	495	750	24.2	1.1
RR Mus	CV2	3090	1.010	-4.34	690	27			SS Vir	CV6	2560	1.080	(-5.05)	560	36	12.5	1.4
Y CVn**	CV5J	2760	1.087	-4.64	260	14	8.5	2.0	DY Dru	CV6	2420	1.150	(-5.05)	900	47		
RU Vir	CV6	2100 ^j		-5.23 ^j	675	230	18.4		RX Cru	CV6	2650		(-5.05)	845	62		
RY Dra	CV5J	2810	1.18	-5.28	550	44	10.0	0.27	RV Cen	CV3	2865 ^k	1.030	-5.51 ^k	940	78	12.6	1.3
NSV6507	CV3	2920		(-4.39)	560	18	6.5	3.1	V996Cen	CV4	2695	1.53	-5.81	830	44	11.0	1.1
Z Lup	CV5	2655	1.12	-5.05	1105	20			X Tra	CV5	2710	1.17	-5.71	460	18	9.1	0.81
AS Cir	CV6	2420		(-5.05)	935	78			U Aps	CV5	2695		-4.68	825	28		
V CrB	CV7	2090		-4.80	845	130	7.5	1.3	V Oph	CV3	3010		-4.25	580	14	7.8	0.64
SU Sco	CV5	2655		(-4.82)	635	22			V1079Sco	CV6	2510	1.10	-5.33	920	120		
V2309Oph ^y	CV6	2425	1.10	(-5.05)	1025	34			TW Oph	CV6	2440	1.20	-5.12	495	23	8.6	0.15
TT Sco	CV6	2430		(-5.05)	865	57			V Pav	CV6	2545		-4.74	430	66	16.0	1.1
SX Sco	CV4	2785		-5.02	830	38			T Dra	CV6	1850		-5.83	1425	820	13.5	1.3
ES Ser	CV6	2500		(-5.05)	905	30			TY Oph	CV5	2680		(-4.82)	845	32		
T Lyr	CV6J	2310	1.29	-5.43	645	80	11.5	2.2	HK Lyr	CV3	2945		-4.66	730	26		
HK Lyr	CV5	2620		-4.39	730	26			DR Ser	CV5	2650		-5.40	1295	100	20.1	3.9
S Sct*	CV4	2755	1.069	-5.18	580	560	17.3		UV Aql	CV5	2700	1.11	-5.01	910	30		
V Aql	CV6	2525	1.25	-5.65	560	66	8.5	1.0	CG Vul	CV5	2685		(-4.82)	805	33		
V1942Sgr	CV2	2960	1.12	-4.60	550	19	10.0	1.1	UX Dra	CV2	3090	1.046	-5.53	545	37	4.0	0.49
AQ Sgr	CV4	2790	1.033	-5.66	790	77	10.0	0.63	V391Aql	CV6	2585		-5.05	1950	38		
TT Cyg*	CV4	2825		-3.98	620	(12:)	13.5		AX Cyg	CV5	2655		-4.03	520	23		
X Sge	CV5	2630		-4.60	860	24			SV Cyg	CV5	2600		-4.22	700	19		
RS Cyg	CV2	3100		-5.08	655	20			RT Cap	CV6	2480	1.10	-4.95	560	23	8.0	1.8
U Cyg	CV5 ^l	2650 ^l		-4.94 ^l	700	100	13.0	1.5	V Cyg	CV7	1880 ^m		-6.28 ^m	740	630	11.5	0.72
T Ind	CV2	2990		-5.36	645	17	6.0	2.0	Y Pav	CV3	2945 ⁿ		-4.84 ⁿ	420	23	8.0	1.4
V1426Cyg	CV7	1975 ^o		(-5.43)	820	540	14.0	1.3	S Cep	CV6	2240 ^p		-5.42 ^p	495	290	22.0	1.2
V460Cyg	CV2	2950	1.062	-5.81	635	45	10.0	0.78	RV Cyg	CV5	2675	1.20	-5.57	640	140	13.5	1.2
LW Cyg	CV5	2580		-5.45	1095	35			RZ Peg	CV3 ^q	2925 ^q		-3.3 ^q	605	10	12.6	0.59
DG Cep	CV2	2985		-4.71	800	23			TX Psc	CV2	3125	1.027	-5.09	315	32	10.7	0.72
WZ Cas	CV2	3095	1.010	-5.48	650	13	3.8	1.0	V688Mon ^u	CV7	1670		(-5.43)	1370	2400	13.4	4.1
FX Ser ^v	CV7	2050		(-5.43)	1230	3100	28.4	0.58	LP And ^w	CV7	2040		(-5.43)	840	2100	14.0	1.7

from Bergeat et al. (2002b, BKR) whose values are astrometric in essence and deduced from HIPPARCOS data (Knapik et al. 1998 and Bergeat et al. 2002a), with no photometric criteria used. The results are shown in Table 1. There is apparently an excellent agreement for the 104 stars of Olofsson et al. (1993a) in common, with 707-708 pc as mean values. A detailed analysis (Bergeat 2004) however proved this is fortuitous since a Malmquist-type bias occurred in the Olofsson et al. distances in this sample of magnitudes $K \leq 2$, adopting $M_K \simeq -8.1$ (actually there is a 3-magnitude range whose central value is close to -7.50). Conversely, no such bias appeared when comparing the distances deduced from the M_K -magnitudes derived by Mennessier et al. (2001) through a maximum likelihood method for 124 carbon giants in common with BKR. There is also a good agreement with BKR in Table 1 for a small sample of 11 stars from Groenewegen et al. (1999). They are located farther away at 1141-1161 pc on average, that is 1.63 times more distant. We also considered a sample of 54 stars in common to Olofsson et al. (1993a) and Schöier & Olofsson (2001). There is a 1.33 ratio (i.e. 1.76 on mass loss rates), in the direction opposite to that of the 3.1 mean ratio of mass loss rates mentioned above. It is to be compared to 0.92 when referred to BKR. The Groenewegen et al. (2002b) mean distance is 2.05 times larger than the BKR-value for 25 stars in common, leading to their mass loss rates being systematically larger. The factor is only 1.35 between Loup et al. (1993) and BKR.

Finally, for the sake of consistency, we transformed the rates \dot{M} given at distances D in the mentioned papers, according to the relation

$$\dot{M}_{\text{BKR}} = \dot{M} (D_{\text{BKR}} / D)^2 \quad (1)$$

where D_{BKR} stands for the distances of Bergeat et al. (2002b). The gas mass loss rates were derived from CO observations by a formula established by Knapp & Morris (1985) for unresolved optically thick envelopes. From a more detailed radiative transfer analysis, Schöier & Olofsson (2001) found that the rates resulting from the formula are systematically underestimated when compared to the new values (their Fig. 8). As expected, the discrepancy increases with decreasing rate i.e. decreasing optical depth. From the comparison of \dot{M}_{BKR} for 53 stars in common we obtained a mean correction factor (f) of 2.5 ± 1.7 to scale the rates from Olofsson et al. (1993a) to the Schöier & Olofsson (2001) level. We adopted mean values in four ranges

$$\begin{aligned} 0.94 \pm 0.34 &\simeq 1 && \text{if } \dot{M}_{\text{BKR}} > 4 \cdot 10^{-6} \\ 2.2 \pm 1.0 &&& \text{if } 4 \cdot 10^{-7} < \dot{M}_{\text{BKR}} < 4 \cdot 10^{-6} \\ 2.5 \pm 1.4 &&& \text{if } 7 \cdot 10^{-8} < \dot{M}_{\text{BKR}} < 4 \cdot 10^{-7} \\ 3.9 \pm 3.1 &&& \text{if } \dot{M}_{\text{BKR}} < 7 \cdot 10^{-8} \end{aligned} \quad (2)$$

where quoted rates refer to values from Olofsson et al. (1993a). This is in fair agreement with Fig. 8 in Schöier & Olofsson (2001). About 70% of the data we used were taken from those two references. From 17 stars in common, we found $f = 1.9 \pm 1.4$ for Groenewegen et al. (2002b, 8%) while $f = 3.3 \pm 0.3$ was deduced from the seven values of Groenewegen et al. (1999, 2.7%). Here too, there is some indication of f tending to unity for objects with very large rates

but we were unable to split the samples. For Loup et al. (1993, 7 stars and 9%), we obtained $f = 1.2 \pm 0.5$ while $f = 3.4 \pm 2.1$ and $f = 3.1 \pm 1.7$ were deduced for Le Bertre et al. (2001, 5 stars) and (2003, 4 stars) respectively. These later five correction factors and those in Eq. (2) were applied to the \dot{M}_{BKR} -data derived from Eq. (1). We rejected the data available in Winters et al. (2003) since the correction factor curiously amounted to 0.4 from only two stars in common with Schöier & Olofsson.

Both the obtained mean gas mass loss rates and the D_{BKR} -distances are given in Table 2 together with photometric groups and effective temperatures from Bergeat et al. (2001). The luminosities in solar units can be derived from the absolute bolometric magnitudes of Bergeat et al. (2002b) making use of

$$L/L_{\odot} = 10^{-0.4(M_b - 4.73)} \quad (3)$$

Additional star identifiers and detailed bibliographic sources of the mass loss data for each star are provided in Table 3, only available in electronic form. The C/O ratios quoted in Table 2 were taken from Lambert et al. (1986), Olofsson et al. (1993b) and Abia & Isern (1996). Also given are the expansion velocities from the same five references mentioned above for mass loss rates. Both the dust and gas mass loss rates are proportional to the adopted squared distance and no corresponding corrections need be applied to the dust-to-gas ratios. The dust mass loss rate is derived from the IRAS (60 μ m) making use of a formula given by Sopka et al. (1985; see e.g. Eq. (8) in Olofsson et al. (1993a). The dust rate is proportional to $L^{-0.5}$. We thus scaled the values from Olofsson et al. (1993b), Groenewegen et al. (1999) and Groenewegen et al. (2002b) to the luminosities quoted in Table 2, according to the individual luminosities adopted by these authors. The obtained values were then divided by the correction factors of Eq. (2) or by 3.3 or 1.9, i.e. the f -factors for the gas mass loss rates from those three references. As discussed in Sect. 7, the latter correction strongly shifts observations toward model predictions. Two estimates are provided by Olofsson et al. (1993a), namely a lower one assuming no drift velocity for the dust, and an upper one adopting an upper limit for drift velocities (up to 20 km/s, i.e. eventually higher than the gas expansion velocity) obtained by equating the radiation force on the grains and the drag force due to gas-grain collisions in the limit of supersonic motion (e.g. Kwok 1975). The estimates from Groenewegen et al. make use of moderate drift velocities, usually 2-3 km/s. Their mean values, $(1.2 \pm 1.3) \cdot 10^{-3}$ for Groenewegen et al. (1999, $n=8$) and $(1.45 \pm 1.1) \cdot 10^{-3}$ for Groenewegen et al. (2002b, $n=24$) are consistent with that of the “lower” values $((1.3 \pm 1.0) \cdot 10^{-3}, n=55)$ of Olofsson et al. (1993a), while the “upper” values yield a significantly larger mean $((3.2 \pm 2.5) \cdot 10^{-3}, n=55)$. Average values of the available data are quoted in Table 2, ignoring the “upper” ones in Olofsson et al. (1993a). They thus correspond to the low drift velocities adopted here.

The sample of Table 2 has 119 carbon-rich giants with at least one of the three quantities from millimetric data given. Many “optical” carbon stars of low to moderate mass loss rates are included while the “infrared” carbon stars with higher rates and often optically thick dust shells are fewer. This is due to our requirement that stellar data be available from Bergeat et

al. (2001, 2002b, 2002c) that, in turn, necessitated sufficient photometric data in the visible range. This is very often missing for “infrared” carbon stars. This is rather unfortunate since 330 “infrared” carbon stars were studied by Groenewegen et al. (2002a, 2002b).

3. The predictions from hydrodynamical models

As mentioned in Sect. 1, both pulsation and dust formation are involved in the mass loss phenomenon on the asymptotic branch. The mass loss relation of Dominik et al. (1990) is based on calculated models and was the first one available. It describes the stationary outflows of carbon-rich low mass stars. *The mass loss rate increases with increasing luminosity and decreasing effective temperature.* The strong dependence upon the effective temperature is due to the fact that dust always condenses at about the same temperature. For stars with higher effective temperatures, this condensation temperature is reached farther out in the shell where dust formation is less effective. *The mass loss rate increases as the stellar mass decreases.* Other things being equal, increased gravity due to larger masses inhibits the wind. The dependence of the mass loss rate on the carbon to oxygen ratio is much less marked, especially for values larger than 1.5. Dominik et al. proposed an analytical fit, their formula (7), which is presumably accurate for extreme mass loss rates, i.e. for $\dot{M} \geq 10^{-6} M_{\odot} \text{yr}^{-1}$. The terminal velocity ranges from 5 to 40 km s⁻¹. *It increases with decreasing effective temperature and with increasing luminosity or increasing C/O ratio.* The authors proposed a linear fit as their Eq. (8). The dust-to-gas density ratio is closely related to the final degree of condensation, as shown by formula (9) of Dominik et al., and it ranges from $6 \cdot 10^{-4}$ to $5 \cdot 10^{-3}$.

Making use of the models of Fleischer et al. (1992) and Fleischer (1994), Arndt et al. (1997) derived a grid of 48 dynamical models usually with less extreme mass loss than in the cases explored by Dominik et al. (1990). They are realistic models of circumstellar dust shells around carbon-rich long-period variables. They include the calculation of time-dependent hydrodynamics as well as a detailed treatment of dust formation, growth and evaporation. The maximum likelihood method was applied to the grid with six parameters they considered as independent, namely the stellar temperature, the stellar luminosity, the stellar mass, the abundance ratio of carbon to oxygen, the pulsational period and the velocity amplitude of the pulsation. They obtained their equations (1), (3) and (5) for the mass loss rate, the dust-to-gas ratio and the expansion (outflow) velocity, respectively. The trends are essentially the same as those obtained by Dominik et al. and summarized above. Keeping constant the parameters of low influence, they also wrote the simplified relations they numbered (2), (4) and (6) for the same three “mass loss” quantities.

Applying a piston and a variable luminosity at the inner boundary in the models of Höfner et al. (1995, 1996), Höfner & Dorfi (1997) constructed a set of 22 carbon-rich LPV models. The ranges of the parameters were smaller but Arndt et al. (1997) conclude a good agreement with their work for values in common.

We recall here the equations (1), (3) and (5) from Arndt et al. (1997) whose predictions we intend to compare with the observed data as collected in Sect. 2. For the mass loss rate in solar mass per year they derived

$$\log \dot{M} = -4.95 - 9.45 \log (T/2600) + 1.65 \log (L/10^4 L_{\odot}) \\ - 2.86 \log (M/M_{\odot}) + 0.47 \log (\epsilon_C/1.8\epsilon_{\odot}) \\ - 0.146 \log (P/650) + 0.449 \log (\Delta u/2.0) \quad (4)$$

where the parameters of major influence are the effective temperature T in Kelvin, the luminosity L and the mass M . The minor parameters are the carbon to oxygen abundance ratio, the period of the LPV in days, and the piston velocity amplitude in km s⁻¹. For the dust-to-gas density ratio, they obtained

$$\log (\rho_d/\rho_g) = 2.74 - 1.62 \log T - 0.248 \log (L/L_{\odot}) \\ - 0.658 \log (M/M_{\odot}) + 2.45 \log (\epsilon_C/\epsilon_{\odot}) \\ + 0.230 \log P - 4.93 \cdot 10^{-3} \log (\Delta u) \quad (5)$$

with the same units. In addition to T , L and M , the carbon to oxygen abundance ratio is here a major parameter. Again, the period and piston velocity amplitude have little influence. Finally, they give for the expansion (or outflow) velocity

$$\log v_{\infty} = 0.730 - 0.148 \log T + 0.107 \log (L/L_{\odot}) \\ - 6.40 \cdot 10^{-2} \log (M/M_{\odot}) + 1.74 \log (\epsilon_C/\epsilon_{\odot}) \\ + 9.56 \cdot 10^{-2} \log P - 7.07 \cdot 10^{-4} \log (\Delta u) \quad (6)$$

where the effective temperature, the luminosity and the carbon to oxygen abundance ratio prove to be the main parameters. The stellar mass, the period of pulsation and the piston velocity amplitude have little influence here.

4. The realm of carbon-rich AGB stars

The adopted values of the six parameters in the models mentioned in Sect. 3 were varied more or less freely by the authors. The resulting Eqs. (4), (5) and (6) are given for ranges of parameter values that are those of the used (satisfactory) models. *Each parameter is supposed to vary independently which is actually not the case for existing carbon-rich giants on the AGB.* We briefly summarize here the results from Bergeat et al. (2001, 2002b, 2002c) and references therein, on this specific topic. The bright carbon-rich giants are located on the asymptotic branch, with various initial masses and chemical compositions. Consequently, those Galactic giants populate a strip in the HR diagram with increasing luminosity for decreasing effective temperature (See Figs. 8 and 9 of Bergeat et al. 2002b). Mean values of both quantities were given in their Table 3 for the HC-CV groups. This classification was shown to be strongly correlated with effective temperature decreasing along the sequence HC0 to HC5 and then CV1 to CV7 (Bergeat et al. 2001). Influenced by true dispersion and errors on distance estimates, the populated strip is rather large but the trend in mean values is obvious. A study of pulsation modes resulted in the evaluation of pulsation masses in good agreement with evolution tracks in the HR diagram (Bergeat et al. 2002c) for long period variables. Mean pulsation masses and

periods increase with decreasing effective temperature along the sequence of photometric groups, as shown in their Table 1. In a mass-luminosity diagram (their Fig. 4), the mean luminosity increases with increasing mean mass. For the cool carbon variables (CV-stars), the carbon to oxygen abundance ratio was plotted against effective temperature in Fig. 7 of Bergeat et al. (2002c). The mean values and dispersions are increasing with decreasing effective temperatures along the CV1 to CV6 sequence. They however decrease below 2500 K at the CV6-CV7 junction, a result possibly due to large dust condensation (SiC and carbonaceous grains) in the atmosphere and resulting carbon depletion in the gas phase. The only parameter of formulae (4) to (6) in Sect. 3 for which we have no indication, is the piston amplitude velocity. It is however supposed to be higher in Miras and semi-regulars with large amplitudes than it is in semi-regulars with low amplitudes and irregular variables. Its influence is however small on the three quantities calculated from Eqs. (4) to (6). We thus adopted the $\Delta u = 2 \text{ km s}^{-1}$ value as favored by Arndt et al. (1997). We have summarized the values in Columns 7 to 9 of Table 4 as calculated from the mean data of Columns 2 to 6, following the same sequence of photometric groups. In those calculations, we eventually went beyond the validity ranges of formulae (4) to (6) *stricto sensu*, as defined by the parameter values that Arndt et al. introduced in their 48 models. Discussions are postponed to the following sections.

5. Mass loss rate vs. effective temperature

The mass loss rates \dot{M} as quoted in Table 2 (Columns 7 and 16) are plotted on a logarithmic scale in Fig. 1 as a function of the effective temperatures from Columns 3 and 12. The main trend of increasing mass loss rate with decreasing effective temperature is observed as expected from theory (Sect. 3). Typical error bars on both coordinates are also shown. The Miras are displayed as crosses while the filled circles stand for semi-regulars. Among the latter, four stars with detached shell(s) are shown with x-symbols in the 2600-2800 K range. Denoted by asterisks in Table 2, they are U Ant, S Sct, R Scl and U Cam. The observation of detached shell(s) is indicative of recent enhanced mass loss. As a consequence, those four stars do exhibit larger mass loss rates than the bulk of our sample, in the same temperature range. Recent observations of a HCN line emission in the central source of R Scl (2625 K) that was resolved were secured with a FWHM of 1" by Wong et al. (2004). The authors thus derive for the *present* mass loss rate $2 \cdot 10^{-7} M_{\odot} \text{ yr}^{-1}$ for an adopted distance of 360 pc, a rate we convert into $3.5 \cdot 10^{-7} M_{\odot} \text{ yr}^{-1}$ for our 475 pc distance estimate (see Column 15 of Table 2). This latter value, displayed as a diamond-symbol in Fig. 1, is located in the main locus. This is about 16 times less than the earlier $5.5 \cdot 10^{-6} M_{\odot} \text{ yr}^{-1}$ value quoted for R Scl in Column 16 of Table 2, a rather drastic change. This is convincing evidence for highly episodic mass loss, possibly caused by a thermal pulse. The detached shell of R Scl has recently been investigated for MgS, mining the mass-loss history of this object (Hony & Bouwman 1998; see also Olofsson et al. 2000 for a detailed study of circumstellar CO in TT Cyg). We conclude that mass loss rates larger than about

Table 4. The mean stellar data for carbon-rich giants (Columns 2-6) from Bergeat et al. (2001, 2002b, 2002c) and the corresponding mass loss data (Columns 7-9) calculated from formulae (4), (5) and (6) taken from Arndt et al. (1997). For photometric groups of Column 1, the mean values of effective temperatures in Kelvin (Column 2), the mean luminosities $l = \langle L/L_{\odot} \rangle$ (Column 3) and masses $m = \langle M/M_{\odot} \rangle$ (Column 4) in solar units, the mean carbon to oxygen abundance ratio C/O (Column 5) and the mean pulsation period P in days (Column 6). The group CV5 “und” corresponds to a small sample of underluminous CV5-stars which are not included. Adopting the piston velocity amplitude $\Delta u = 2 \text{ km s}^{-1}$ favored by Arndt et al., the corresponding mass loss rates $\dot{M}' = 10^7 \dot{M}$ (Column 7) where \dot{M} is in solar mass per year, the dust-to-gas abundance ratios $\rho_{d/g} = 10^4 \rho_d/\rho_g$ (Column 8) and the expansion velocities v_e in km s^{-1} (Column 9).

G	T_{eff}	l	m	C/O	P	\dot{M}'	$\rho_{d/g}$	v_e
HC5	3470	1735	0.57 ± 0.20	1.01 ± 0.01	290 ± 70	1.7	8.6	6.5
CV1	3290	2265	0.55 ± 0.15	1.005 ± 0.01	299 ± 98	5.4	9.2	6.7
CV2	3095	4130	1.0 ± 0.2	1.01 ± 0.01	339 ± 71	5.2	6.3	7.1
CV3	2920	4885	1.6 ± 0.3	1.03 ± 0.03	355 ± 73	2.7	5.0	7.3
CV4	2775	5960	1.9 ± 0.35	1.13 ± 0.13	353 ± 55	3.7	5.7	8.8
CV5	2640	6530	2.6 ± 0.5	1.2 ± 0.2	389 ± 40	2.7	5.8	9.8
CV5 und	2645	1600	0.5:		423:			
CV6	2435	8635	4.2 ± 0.8	1.4 ± 0.4	448 ± 53	2.5	6.9	13.4
CV7	1950	16445	8.2:	1.4: ± 0.4	444: ± 107	8.7	5.3	13.9
CV7	1950	16445	4.2	1.4:	444:	62	8.4	14.5

$10^{-6} M_{\odot} \text{ yr}^{-1}$ in the 2500-2800 K range are representative of temporarily-enhanced mass loss leading to detached shell(s) hundreds or a few thousands of years later (see e.g. Lindqvist et al 1996 for U Cam, Izumiura et al. 1997 for U Ant, Izumiura et al. 1996 and Le Bertre & Gérard 2004 for Y CVn).

At lower temperatures, we used symbols surrounded by squares for five stars with optically-thick dust shells as shown by large infrared excesses. They are CW Leo (IRC+10216), V 346 Pup and LP And (three Miras), and RW LMi (CIT 6) and FX Ser (two semi-regulars). They exhibit mass loss rates much larger than those from the carbon-rich giants with optically-thin dust shells in the same 2500-1800 K range, that is larger than about $6 \cdot 10^{-6} M_{\odot} \text{ yr}^{-1}$ for effective temperatures less than 2500 K. A few intermediate objects are also noticed (V Hya, BN Mon). The circumstellar envelope characteristics of 9 carbon stars were probed by Schoier et al. (2002), combining radio measurements and infrared observations from ISO. Their radiative transfer analysis allowed us to put constraints on the mass loss history of those objects, specially CW Leo=IRC+10216 and RW LMi=CIT6 (studied here) and IRAS 15194-5115=II Lup=CGCS 3592 (not included). They found that those stars are not likely to have experienced any drastic long-term mass loss rate modulations, at least less than a factor of about 5, over

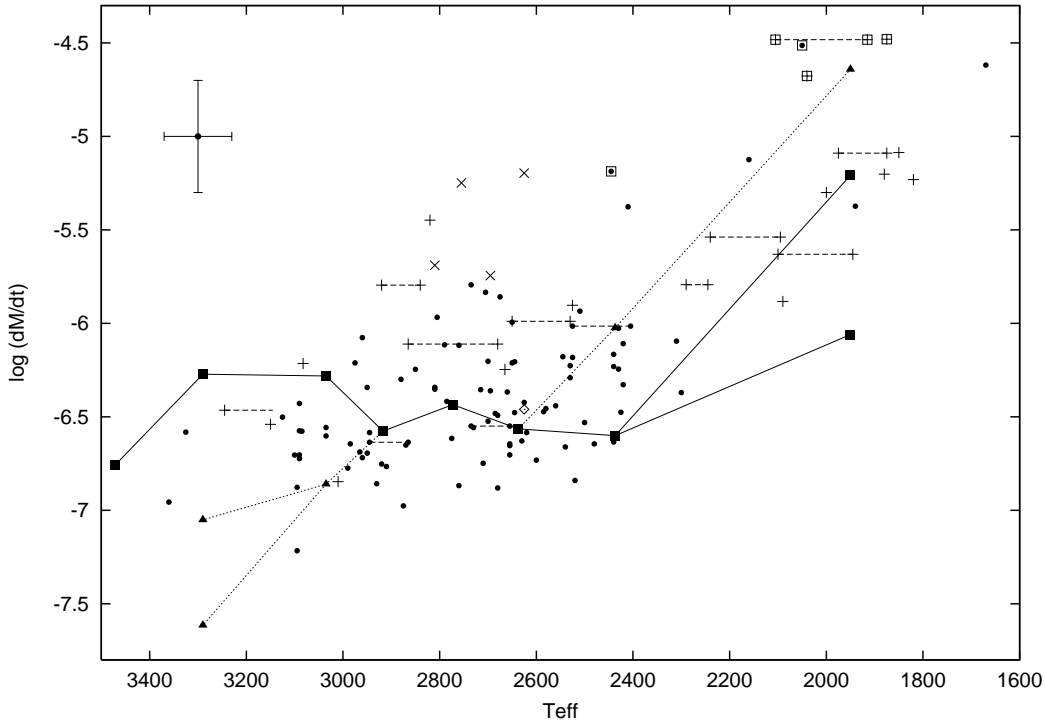


Fig. 1. Logarithm of the mass loss rate in solar mass per year as a function of effective temperature in Kelvin, as taken from Table 2 (observations). Typical error bars are displayed at left. Semi-regulars and Miras are shown as filled circles and crosses respectively with 4 non-Miras with detached shells (\times and diamond symbol for present R Scl), and 5 objects with optically-thick dust shells (squared symbols). For a few variables, there are two symbols for temperatures obtained at distinct phases. The predictions from models (Table 4) are plotted as filled squares connected by full lines. Additional predictions for various mean masses are shown as filled triangles connected with dashed lines (see text).

the past thousands of years. This is a situation in contrast with the case of the detached shells mentioned above.

If we remove the nine symbols of those high mass loss objects in Fig. 1, the remaining filled circles (semi-regulars) and crosses (Miras) populate a locus with a flat portion in the 2900-2400 K range and for $n=66$ stars,

$$\log \dot{M} \simeq (-0.8 \pm 1.7) \log T_{\text{eff}} - (3.6 \pm 5.8) \quad (7)$$

with an average value of

$$\langle \dot{M} \rangle \simeq (5.8 \pm 4.4) 10^{-7} M_{\odot} \text{yr}^{-1} \quad (8)$$

for this wide $10^{-7} - 2 \cdot 10^{-6} M_{\odot} \text{yr}^{-1}$ nearly horizontal strip. It is flanked by two ranges of increasing mass loss rate with decreasing effective temperature. For $T_{\text{eff}} \geq 2900$ K we obtain for 32 stars

$$\dot{M} \simeq 4.51 10^{20} T_{\text{eff}}^{-7.83} M_{\odot} \text{yr}^{-1} \quad (9)$$

and for $T_{\text{eff}} \leq 2400$ K with 17 stars

$$\dot{M} \simeq 8.46 10^{24} T_{\text{eff}}^{-9.20} M_{\odot} \text{yr}^{-1} \quad (10)$$

Those three relations which are not satisfied by the 9 objects with strong mass loss and possibly a few others, are not shown in Fig. 1. Instead the predictions of Sect. 4 as quoted in Table 4 are plotted as filled square-symbols connected by a full broken line. A very good agreement is observed in the 3000-2400 K

range of effective temperatures and the observed flat portion is confirmed by the predictions. We shall identify its cause later in this section. Below 2400 K, the observed locus is well reproduced by predictions provided $M = 4.2 M_{\odot}$ is adopted instead of the uncertain $M = 8.2 M_{\odot}$ value estimated by Bergeat et al. (2002c) from a few extreme objects. This high value was possibly induced by overestimating the “photospheric” radius of very cool giants with dust shells. The right portion of Fig. 1 is an additional argument in favor of masses not exceeding about $4 M_{\odot}$ for a large majority of luminous carbon-rich giants. For effective temperatures higher than 3000 K, there is an increasing disagreement between observations and predictions up to 3400 K. Hot variables exhibit an irregular pulsational behaviour with small amplitudes, resulting in dubious pulsation mode and period. Uncertainties increase accordingly. It should be noted that, according to Arndt et al. (1997), one has to refrain from applying Eqs. (4) to (6) beyond 3000 K since none of their 48 models lies there. In addition, none of their models is fainter than $5 \cdot 10^3 L_{\odot}$ contrary to the observed averaged mean luminosities of HC5, CV1 and CV2-stars in Table 4. We however attempted to apply the $\langle M \rangle = 1.6 M_{\odot}$ mean value of the CV3-group in Table 4 to the other earlier groups CV1 and CV2 with other data otherwise unchanged. Together with an additional calculation from Eq. (4) assuming for CV1 the $\langle M \rangle = 1.0 M_{\odot}$ value quoted for CV2 in Table 3, they are plotted as filled triangles in Fig. 1. The dashed lines connecting the

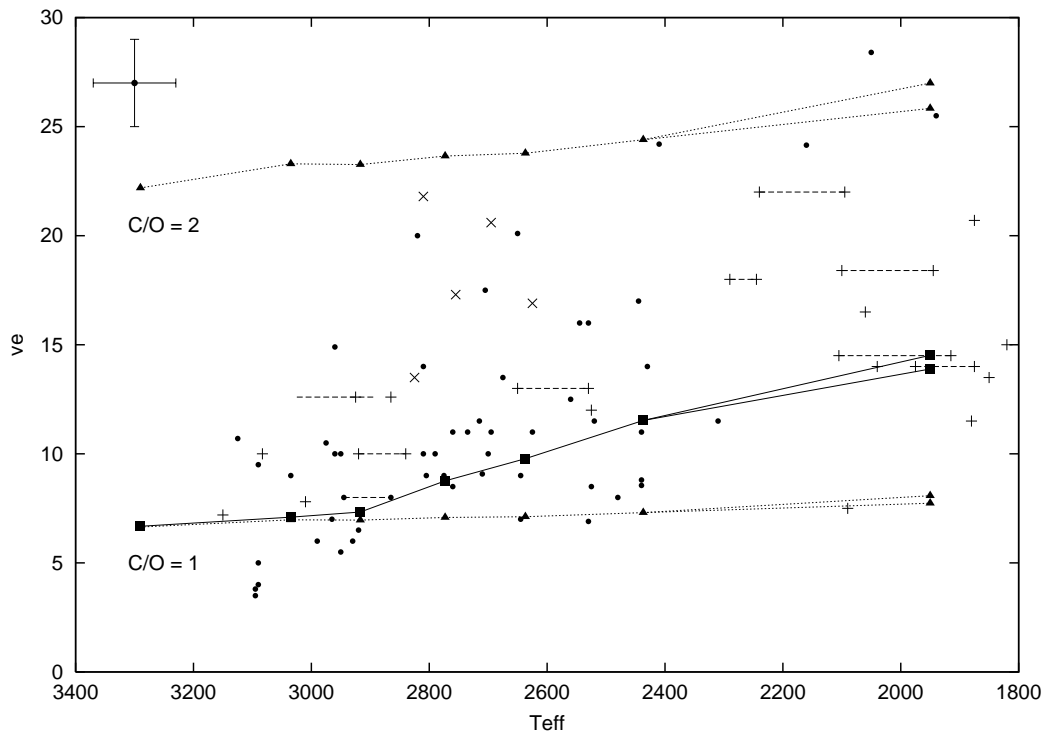


Fig. 2. Outflow (expansion) velocities in km/s as a function of effective temperatures in Kelvin, as taken from Table 2 (observations) and Table 4 (predictions from models). Typical error bars are also displayed at left. Same symbols used as in Fig. 1, with 5 non-Miras with detached shells (\times). The predictions from theory are plotted as filled squares connected by full lines. Extreme lines corresponding to $C/O=1$ and $C/O=2$ respectively are also shown (see text).

CV3-square to the filled triangles for CV1 and CV2 and the initial segmented full line reasonably well encompass the observations. This result suggests that the slope for $T_{\text{eff}} > 2900$ K in Fig. 1 is indicative of a nearly uniform value of about one solar mass. A large correction factor (3.9 or 2.5) from Eq. (2) was applied to part of the contributing data. Without that correction, the shift of observations below the continuous line of predictions would have been substantially larger. Similarly the slope below 2400 K seems to correspond to a nearly uniform value of about $4 M_{\odot}$. The latter is predicted as the upper limit from evolutionary calculations presumably due to hot bottom-burning most effective in AGB stars of larger masses (Bergeat et al. 2002b and references therein). We also calculated the mass loss rate of the CV6 and CV7-groups, assuming the $\langle M \rangle = 2.6 M_{\odot}$ value quoted for CV5 in Table 3, keeping the other parameters unchanged. They are shown as filled triangles connected to the CV5-square by a broken dashed line. A possible explanation of higher mass loss rate might be smaller mass due to previous strong mass loss. Precisely, Schoer et al. (2002) deduced that mass loss rates remained high over the past thousands of years in objects like CW Leo=IRC+10216 and RW LMi=CIT6. From the comparison of theoretical nucleosynthesis models and measurements of abundances in the circumstellar envelope, Kahane et al. (2000) favor a mass not larger than $2 M_{\odot}$ for CW Leo, well below the $4.2 M_{\odot}$ -limit considered for the stars of Eq. (10). Winters et al. (1994a) previously estimated $M \leq 2 M_{\odot}$ with $C/O \approx 1.4$ for CW Leo. In other words, the apparent (lasting) “superwinds” could well be

standard mass loss in objects of diminished masses. It should be noted that Arndt et al. (1997) did not calculate models cooler than 2300 K. Additional data and models are clearly necessary before a firm conclusion can be reached.

We shall see in Sect. 6 that the four stars with detached shells mentioned above also have expansion velocities larger than average. Actually, it happens that velocities are little influenced by adopted masses (Sects. 3 and 6). In addition, R Scl has now returned to low mass loss rates (Wong et al. 2004). For those stars with detached shells and intermediate (2400-2900 K) effective temperature, the above explanation of enhanced mass loss in terms of diminished masses is not acceptable. By continuity, we are led to the conclusion that the 3000-2400 K flat portion corresponds to the approximate $1 - 4 M_{\odot}$ mass range. Discussing their formula (1), i.e. our Eq. (4), Arndt et al. (1997) concluded that the abundance ratio, pulsation period and piston amplitude velocity have only small influences on the mass loss rate. Accordingly, we find no clear difference between the loci of Miras and semi-regulars. It remains to consider the effective temperature, the luminosity and the mass of the star. Since, on average, luminosity increases with decreasing effective temperature, both parameters contribute to an increase of the mass loss rate. Following Eq. (4), that increase is inhibited in the 3000-2400 K range by the increase of stellar mass in the $1 - 4 M_{\odot}$ domain. *The 3000-2400 K flat portion in Fig. 1 is a further argument in favor of the $1 - 4 M_{\odot}$ range for bright carbon-rich giants (less luminous objects can populate the $0.5 - 1 M_{\odot}$ domain), in addition to the use of evolutionary*

tracks in the HR diagram and to the calculations of present pulsation masses (Bergeat et al. 2002b, 2002c). We conclude that the models and relations from Arndt et al. (1997) satisfactorily reproduce the mass loss rate deduced from millimetric observations. Larger mean mass thus implies, other things being equal, a lower mass loss rate.

6. Outflow velocity vs. effective temperature

The outflow or expansion velocities v_e , i.e. estimates of velocity at infinity in km/s as quoted in Table 2 (Columns 8 and 17) are plotted in Fig. 2 as a function of the effective temperatures from Columns 3 and 12. The main trend of increasing expansion velocity with decreasing effective temperature is observed as expected from theory (Sect. 3), but with a large scatter here. Typical error bars on both coordinates are also shown and are much smaller. The same symbols as in Fig. 1 are used. The \times -symbols point to five stars with detached shells (U Ant, S Sct, R Scl, U Cam and TT Cyg). The latter also show large velocities (14-21 km/s) for $T_{\text{eff}} \simeq 2600 - 2800$ K about a factor 2 larger than predicted values. We already found in Sect. 5 that they display higher mass loss rates than predicted. The issue is dubious for the five cool extreme objects of Sect. 5. They are scattered with CW Leo=IRC+10216 on the predicted relation and FX Ser located well above it.

The predictions of v_∞ from Eq. (6) as quoted in Table 4, are shown in Fig. 2 as filled square-symbols connected by a broken full line. The latter fits reasonably well the 86 % of the stars in the sample that are located in the lower part of the diagram. The models seem to correctly predict the low expansion velocities which roughly correspond to the low mass loss rates of Sect. 5, themselves well-predicted by the same models. The decreasing effective temperature and increasing luminosity along the sequence of Table 3 both contribute to the increase of the outflow velocity but the effect is small when compared to the influence of the ϵ_C/ϵ_O abundance ratio. This point is illustrated by the two dashed lines in Fig. 2 as obtained keeping the ratio to 1 or 2 instead of the mean values of Table 4. Within errors, the observed values lie between those two lines. This is precisely the range of the abundance ratio as derived from spectra and model atmospheres of the cool carbon-rich giants (Lambert et al. 1986 and references cited in Sect. 2; see also Fig. 7 of Bergeat et al. 2002c).

We also note that above 2900 K the observations in Fig. 2 tend to concentrate towards the C/O=1 line, below 10-15 km/s. This can be attributed to the fact that stars in the hotter domain of Table 4 do have mean abundance ratios close to unity with a small range apart. Below 2900 K (CV3 and later groups), the C/O mean values and ranges increase (Table 4). On average, larger velocities are reached there. The influence of the C/O ratio is responsible for a triangular void in Fig. 2 at $T_{\text{eff}} \geq 2800$ K that is inserted between the C/O=1 and C/O=2 lines. Predictions are consistent with millimetric observations and visible and infrared spectroscopy with $1 \leq \epsilon_C/\epsilon_O \leq 2$, and with the mean values and dispersions as functions of effective temperature from Bergeat et al. (2001), as displayed in Fig. 7 of Bergeat et al. (2002c).

7. Dust-to-gas ratio vs. effective temperature

The diagram of the dust-to-gas ratio against effective temperature is not shown here. There is actually no marked slope when Eq. (5) and the corresponding predictions of Table 4 are used. In the 2300-3000 K validity domain of models from Arndt et al. (1997), the mean value amounts to

$$\langle \rho_{d/g} \rangle = \langle \rho_d/\rho_g \rangle \simeq (5.9 \pm 0.7) 10^{-4} \quad (11)$$

As described in Sect. 2, the mean observed values quoted in Table 2 are typically “lower” ones derived assuming low drift velocities. For 72 documented stars, we obtained

$$\dot{M}_d/\dot{M}_g \simeq (1.3 \pm 1.1) 10^{-3} \quad (12)$$

a value about 2.2 times larger than the predicted one. There is practically no slope in the diagram of “observed” dust-to-gas ratios of rates against effective temperatures from Table 2, at least within the large error bars. It must be emphasized here that the data used was corrected for the f-factor of Sect. 2 and for a smaller factor for adopted luminosity

$$\left(\dot{M}_d/\dot{M}_g\right)_{\text{BKR}} = \left(\dot{M}_d/\dot{M}_g\right)_{\text{Lit}} \left(L_{\text{BKR}}/L_{\text{Lit}}\right)^{-0.5} \quad (13)$$

Without that f-correction, the above discrepancy ratio would have jumped from 2.2 to about 6. The mean “upper” value of $(3.2 \pm 2.5) 10^{-3}$ derived in Sect. 2 is about 5.4 times larger than the Eq. (11) predicted value. Apparently, adopting larger drift velocities could make the discrepancy between observations and predictions even worse, but predicted values would also be increased. Very recent models with the influence of the grain drift velocity properly treated (Sandin & Höfner 2004) can contribute to shift predictions closer to observations. The derivation of the ratio from the observations makes use of data from both infrared and millimetric ranges, with simplifying assumptions (like a unique temperature for instance). It is not clear whether the same layers are involved in the extended atmosphere and shell (from inner dust condensation zone to outer regions with terminal velocity reached).

Following Eq. (5) taken from Arndt et al. (1997), it appears that in addition to decreasing effective temperature and increasing luminosity whose influences counteract here, the stellar mass and the ϵ_C/ϵ_O abundance ratio do have an appreciable influence. The predicted dust-to-gas density ratio increases with both decreasing stellar mass and increasing abundance ratio. Adopting for instance $M = 1 M_\odot$ and $\epsilon_C/\epsilon_O \geq 2$ can rise the Eq. (11) value higher than that in Eq. (12), reaching the level of the highest “lower” values observed. It seems outside the range of acceptable parameter values taking into account the analyses of Sects. 5 and 6 from Table 4 data. However, keeping the mass range of Table 4 that fits nicely the gas mass loss rate data (Sect. 5), an increase of about 20% of the C/O ratios from Lambert et al. (1986) can help, which remains compatible with the velocity comparison in Fig. 2. Their abundance ratios for 30 carbon stars lead to $\langle (^{12}\text{C} + ^{13}\text{C})/H \rangle \simeq (5.5 \pm 1.6) 10^{-4}$ in numbers of atoms and $(2.7 \pm 1.0) 10^{-3}$ in mass for a gas principally of H and He, if their C/O ratios are kept. The estimate is then of 22% of carbon locked up in grains if prediction of Eq. (11) is trusted against 48% for the mean observed ratio of Eq. (12). If confirmed, such figures would mean that carbon molecules could

be appreciably depressed. Very high drift velocities could lead to unreasonably high estimates.

8. Discussion and conclusions

We have compared the results of millimetric (and infrared) observations, namely gas mass loss rate, expansion (outflow) velocity and dust-to-gas density ratio, to the predictions from hydrodynamical time-dependent models of dust-driven winds for carbon-rich chemistry. Corrections were applied to the published “observed” values of the first (distance and radiative transfer) and the third quantity (luminosity and radiative transfer) as described in Sect. 2. The prediction of models are applied to long period variables whose pulsation is simulated by a piston of given amplitude velocity and period acting at the basis of the atmosphere. We made use of the approximate formulae of Arndt et al. (1997) based on 48 models exploring ranges in the six parameters they include. Among them, the pulsation period and the piston amplitude velocity have only little influence (Sect. 3). We found no marked difference in the observed data between Miras and non-Miras (here semi-regulars with available periods). Four parameters remain whose ranges may influence the results, namely effective temperature taken as the stellar temperature used in the models, luminosity, mass and carbon to oxygen abundance ratio. The observational data was summarized in Table 2 for 119 carbon-rich giants formerly studied by Bergeat et al. (2001, 2002b and 2002c), for effective temperatures, luminosities, stellar masses and C/O abundance ratio. The formulae (4), (5) and (6) as taken from Arndt et al. lead for the mean values of Bergeat et al. to the estimated means of Table 4 for the samples corresponding to the photometric groups HC5 and CV1 to CV7 with a range of effective temperatures from 3470 K down to 1950 K. This latter parameter is considered as the most accurate one at present and it is used for reference. We also hold fixed to reference values the stellar mass and the C/O abundance ratio keeping unchanged the run of effective temperatures and luminosities of Table 4, namely the TP-AGB of Galactic carbon-rich giants in the HR diagram, as obtained by Bergeat et al. (2002c).

As described in Sect. 5, we obtained a good agreement between predictions and observations in the diagram of mass loss rate vs. effective temperature (Fig. 1). For about 90% of our sample, the mechanism involving gas lifted by pulsation and radiation pressure on condensed dust is confirmed. Three equations (7) and thus (8), (9) and (10) were obtained in the three ranges of effective temperatures distinguished. The usual statement (van Loon et al. 2003) that $\dot{M} \propto T_{\text{eff}}^{-8}$ is approximately true only above 2900 K (Eq. (9)) and below 2400 K (Eq. (10)), with different proportionality coefficients however. There is practically no variation over the 2400-2900 K range in Fig. 1 (including about 55% of our sample). *Predictions and observations are in agreement provided the variations of luminosity on the AGB in the HR diagram (Bergeat et al. 2002b) and the mean masses ranging from about $1M_{\odot}$ around 3000 K to about $4M_{\odot}$ around 2400 K (see Table 4), as deduced from theoretical tracks in the HR diagram and from pulsations masses (Bergeat et al. 2002c).* Here mass is the third important parameter, with influence much larger than that of the C/O abundance ratio. At

low effective temperatures, Eq. (10) corresponds to a constant mass of about $4M_{\odot}$. At high temperatures, Eq. (9) describes carbon variables of about $1M_{\odot}$ or less, but both observations and predictions are uncertain there. Nine giants in our sample (at least) do have mass loss rates larger than predicted from Eqs. (7) to (10). Four cases of detached shells are found in the 2600-2800 K range, i.e. objects having experienced highly episodic mass loss possibly caused by a thermal pulse. One of them (R Scl) has returned to a moderate mass loss rate (Wong et al. 2004), and this is certainly true for the others (e.g. Olofsson et al. 2000 for TT Cyg). This is a strong argument in favor of a specific mass loss mechanism at work. The other five stars are very cool objects with $T_{\text{eff}} \leq 2500\text{K}$ and optically-thick dust shells shown by strong infrared excesses, a consequence of very high mass loss rates, like RW LMi (CIT6) or CW Leo (IRC+10216). Schoier et al. (2002) have shown that the gas mass loss rate of those extreme objects did not vary much over the last thousand of years. As argued in Sect. 5, they may be stars with masses of about $1.5 - 2.5M_{\odot}$, in contrast with the $4.2M_{\odot}$ favored for the cool objects with lower rates as given by Eq. (10). If true, no specific mass loss mechanism would be required here, contrary to the case of detached shells.

A good agreement is also obtained between predictions and observations in the diagram of expansion (outflow) velocity vs. effective temperature (Fig. 2), as described in Sect. 6. The expansion (outflow) velocity increases with decreasing effective temperature, with about 86 % of the objects within the range of predictions as quoted in Table 4 from Eq. (6). To within error bars, the observations are located between the two lines obtained for $\epsilon_{\text{C}}/\epsilon_{\text{O}} = 1$ and $\epsilon_{\text{C}}/\epsilon_{\text{O}} = 2$ respectively, the other parameters being kept equal to their values in Table 4 (including the mean mass distribution successfully used for mass loss rates and described above). This is the range deduced from spectroscopy and model atmospheres (Lambert et al. 1986; see also Fig. 7 of Bergeat et al. 2002c). In Fig. 2, it is remarkable that for effective temperatures higher than about 2900 K, the stars concentrate towards the $\epsilon_{\text{C}}/\epsilon_{\text{O}} = 1$ line, below 10-15 km/s. The maximum observed velocity rapidly decreases with increasing temperature, leaving empty a large triangular area in Fig. 2. The result of Bergeat et al. (2001, Fig. 7 in 2002b) is confirmed that above 2900 K, the C/O ratio remains close to unity with little dispersion. The $\epsilon_{\text{C}}/\epsilon_{\text{O}}$ abundance ratio is confirmed here as the third major parameter with effective temperature and luminosity, while stellar mass has little influence in Fig. 2. Cases of superwind however blur the information from that figure. *We conclude that both mass loss rates and outflow velocities are correctly modeled from recent hydrodynamical calculations of dust-driven winds. Both the levels and the dependence on effective temperature are fairly well reproduced.*

Both the predicted and observed ratios of dust-to-gas mass loss rates show little variation with effective temperature if any. As found in Sect. 7, the average observed value of $\langle \dot{M}_{\text{d}}/\dot{M}_{\text{g}} \rangle \simeq (1.3 \pm 1.1) 10^{-3}$ is a factor 2.2 larger than the mean predicted value $\langle \rho_{\text{d/g}} \rangle = \langle \rho_{\text{d}}/\rho_{\text{g}} \rangle \simeq (5.9 \pm 0.7) 10^{-4}$ from Eq. (5). We have discussed in Sect. 7 the influence of the stellar mass and C/O abundance ratio. It should be noted that the uncertainties are very large here. Among the possible explanations is a moderate underestimate of abundance ratios (say

20%) from model atmospheres, the overall agreement of Fig. 2 being preserved. Another explanation of the above-mentioned disagreement might be some phenomenon in the micro-physics of dust grains, especially the non-equilibrium dust formation process (Andersen et al. 2003, Sandin & Höfner 2004 and references therein). Allowing drift in the time-dependent (grain growth) wind models alters their structure. In some cases there is several times more dust in drift models than in non-drift ones, even at low drift velocity (a few km/s). It is also found that drift plays an active role in accumulating dust to certain narrow regions (Sandin & Höfner 2004), which renders the above comparison even more difficult. It was however seen in Sect. 7 that element abundances from model atmospheres raise constraints limiting the magnitude of such effects. Further investigations are needed before we can determine which estimate is closer to truth.

We finally give in Appendix A a few simple approximate formulae in a parametric form. They reproduce the results of the present study with fairly good accuracy. They can be useful for readers wishing not to enter into the full details of the present analysis.

Acknowledgements. We gratefully acknowledge constructive criticism and valuable suggestions from an anonymous referee. Our analysis was improved and a few points clarified.

Appendix A: Approximate formulas

Some readers may wish not to enter into the full details of the present analysis. From Eq. 6 and Fig. 2, we propose for the expansion velocities

$$\log v_{\infty} = (-0.219 \pm 0.012) \log T_{\text{eff}} + (1.603 \pm 0.041) + 1.74 \log(\epsilon_{\text{C}}/\epsilon_{\text{O}}) \quad (\text{A.1})$$

for $T_{\text{eff}} \leq 3150$ K, and for $T_{\text{eff}} \geq 3150$ K,

$$\log v_{\infty} = (-0.682 \pm 0.056) \log T_{\text{eff}} + (3.219 \pm 0.198) + 1.74 \log(\epsilon_{\text{C}}/\epsilon_{\text{O}}) \quad (\text{A.2})$$

where the first two terms include the data in Table 4 concerning the other (minor) parameters. Concerning the mass loss rates (Eq. (4) and Fig. 1), we can write

$$\log \dot{M} = (-14.62 \pm 0.18) \log T_{\text{eff}} + (44.66 \pm 0.60) - 2.86 \log(M/M_{\odot}) \quad (\text{A.3})$$

for $T_{\text{eff}} \leq 2900$ K, and for $T_{\text{eff}} \geq 2900$ K,

$$\log \dot{M} = (-19.12 \pm 0.44) \log T_{\text{eff}} + (60.21 \pm 1.53) - 2.86 \log(M/M_{\odot}) \quad (\text{A.4})$$

For the dust-to-gas density ratio, the observations point to $\langle \rho_{\text{d}}/\rho_{\text{g}} \rangle = \langle \rho_{\text{d}}/\rho_{\text{g}} \rangle \simeq (1.3 \pm 1.1) 10^{-3}$ while predictions from Eq. (5) can be written as

$$\log(\rho_{\text{d}}/\rho_{\text{g}}) = (1.630 \pm 0.268) \log T_{\text{eff}} + (-9.007 \pm 0.906) + 2.45 \log(\epsilon_{\text{C}}/\epsilon_{\text{O}}) \quad (\text{A.5})$$

for $T_{\text{eff}} \leq 2775$ K, and for $T_{\text{eff}} \geq 2775$ K,

$$\log(\rho_{\text{d}}/\rho_{\text{g}}) = (4.635 \pm 0.605) \log T_{\text{eff}} + (-19.35 \pm 2.10) + 2.45 \log(\epsilon_{\text{C}}/\epsilon_{\text{O}}) \quad (\text{A.6})$$

The mean effective temperatures and luminosities (in solar units) of Table 4 follow the relation

$$\log l = (-3.065 \pm 0.100) \log T_{\text{eff}} + (14.31 \pm 0.34) \quad (\text{A.7})$$

for $T_{\text{eff}} \leq 3050$ K, and for $T_{\text{eff}} \geq 3050$ K,

$$\log l = (-6.528 \pm 0.693) \log T_{\text{eff}} + (26.34 \pm 2.43) \quad (\text{A.8})$$

two relations where the true dispersion in the H-R diagram is not taken into account. The mass-luminosity relation in Table 4 was described in detail in Sect. 6 of Bergeat et al. (2002c; their equations (10) to (12)). In solar units, we obtain

$$\log l = (0.72 \pm 0.07) \log m + (3.58 \pm 0.12) \quad (\text{A.9})$$

for the whole range $0.5 - 4.2 M_{\odot}$ or $3500-2300$ K. Restricting ourselves to the best-documented region from CV2 to CV5 ($3150-2550$ K) roughly corresponding to $1 - 3 M_{\odot}$, we derive

$$\log l = (0.497 \pm 0.075) \log m + (3.658 \pm 0.034) \quad (\text{A.10})$$

that is nearly

$$l \propto m^{1/2} \quad (\text{A.11})$$

References

- Abia, C., & Isern, J. 1996, *ApJ*, 460, 443
- Alksnis, A., Baklaus, A., Dzervitis, U., et al., 2001, *Baltic Astronomy*, 10, 1, third (electronic) ed. of Stephenson's 1989 catalogue at <http://www.astr.lu.lv/>
- Andersen, A.C., Höfner, S., & Gautschy-loidl, R. 2003, *A & A*, 400, 981
- Arndt, T.U., Fleischer, A.J., & Sedlmayr, E. 1997, *A & A*, 327, 614
- Bergeat, J. 2004, in preparation for *A & A*
- Bergeat, J., Knapik, A., & Rutily, B. 2001, *A & A*, 369, 178
- Bergeat, J., Knapik, A., & Rutily, B. 2002a, *A & A*, 385, 94
- Bergeat, J., Knapik, A., & Rutily, B. 2002b, *A & A*, 390, 967
- Bergeat, J., Knapik, A., & Rutily, B. 2002c, *A & A*, 390, 987
- Blöcker, T. 1995, *A & A*, 297, 727
- Dominik, A.J., Gail, H.-P., Sedlmayr, E., & Winters, J.M. 1990, *A & A*, 240, 365
- ESA, 1997, *The HIPPARCOS Catalogue*, ESA SP-1200 (ESA)
- Fleischer, A.J., 1994, *Hydrodynamics and Dust Formation in the Circumstellar Shells of Miras and Long-Period Variables*, PhD thesis, Technische Universität, Berlin, FRG
- Fleischer, A.J., Gauger, A., & Sedlmayr, E. 1992, *A & A*, 266, 321
- Gail, H.-P., & Sedlmayr, E. 1988, *A & A*, 206, 153
- Groenewegen, M.A.T., Baas, F., Blommaert, J.A.D.L., et al. 1999, *A & AS*, 140, 197
- Groenewegen, M.A.T., Sevenster, M., Spoon, H.W.W., & Pérez, I. 2002a, *A & A*, 390, 501
- Groenewegen, M.A.T., Sevenster, M., Spoon, H.W.W., & Pérez, I. 2002b, *A & A*, 390, 511
- Höfner, S., Feuchtinger, M., & Dorfi, E.A. 1995, *A & A*, 297, 815
- Höfner, S., Fleischer, A.J., Gauger, A., et al. 1996, *A & A*, 314, 204
- Höfner, S., & Dorfi, E.A. 1997, *A & A*, 319, 648
- Hony, A., & Bouwman, J. 2004, *A & A*, 413, 981
- IRAS Point Source Catalogue, version 2, 1988, Joint IRAS Science Working Group, vols. 2 to 6, NASA RP-1190, Washington D.C.: U.S. Government Printing Office (IRAS)
- Izumiura, H., Hashimoto, O., Kawara, K., Yamamura, I., & Waters, L.B.F.M. 1996, *A & A*, 315, L221

- Izumiura, H., Waters, L.B.F.M., de Jong, T., et al. 1997, A & A, 323, 449
- Kahane, C., Dufour, E., Busso, M. et al. 2000, A & A, 357, 669
- Kholopov, P.N., Samus, N.N., Frolov, M.S., et al., 1985 General Catalogue of Variable Stars. Nauka Publishing House, Moscow (GCVS). New edition as an electronic version at the Sternberg Institute in Moscow (ftp sai.msu.su with anonymous as user and email address as pw).
- Knapik, A., Bergeat, J., & Rutily, B. 1998, A & A, 334, 545
- Knapp, G.R., & Morris, M. 1985, ApJ, 292, 640
- Kwok, S., 1975, ApJ, 198, 583
- Lambert, D.L., Gustafsson, B., Erikson, K., & Hinkle, K.H. 1986, ApJS, 62, 373
- Le Bertre, T., Matsuura, M., Winters, J.M., et al. 2001, A & A, 376, 997
- Le Bertre, T., Tanaka, M., Yamamura, I., & Murakami, H. 2003, A & A, 403, 943
- Le Bertre, T., & Gérard, E. 2004, A & A, 419, 549
- Lindqvist, M., Lucas, R., Olofsson, H., et al. 1996, A & A, 305, L57
- Loup, C., Forveille, T., Omont, A., & Paul, J. 1993, A & AS, 99, 291
- Mamon, G.A., Glassgold, A.E., & Huggins, P.J. 1988, ApJ, 328, 797
- Meixner, M., Campbell, M.T., Welch, W.J., & Likkell, J. 1998, ApJ, 509, 392
- Menessier, M.-O., Mowlavi, N., Alvarez, R., & Luri, X. 2001, A & A, 374, 968
- Olofsson, H., Erikson, K., Gustafsson, B., & Carlström, U. 1993a, ApJS, 87, 267
- Olofsson, H., Erikson, K., Gustafsson, B., & Carlström, U. 1993b, ApJS, 87, 305
- Olofsson, H., Bergman, P., Lucas, R., et al., 2000, A & A, 353, 583
- Reimers, D. 1975, In *Problèmes d'Hydrodynamique Stellaire*, Mem. Soc. R. Sci. Liège, 6^e, 8, 369
- Sandin, C., & Höfner, S. 2004, A & A, 413, 789
- Schoier, F.L., & Olofsson, H. 2000, A & A, 359, 586
- Schoier, F.L., & Olofsson, H. 2001, A & A, 368, 969
- Schoier, F.L., Ryde, N., & Olofsson, H. 2002, A & A, 391, 577
- Skinner, C.J., Meixner, J., & Bobrowsky, M. 1998, MNRAS, 300, L29
- Sopka, R.J., Hildebrand, R.H., Jaffe, D.T., et al. 1985, ApJ, 294, 242
- Stephenson, C.B., 1989, Pub. of the Warner & Swasey Obs. 3, No 2
- van Loon, J.Th., Marshall, J.R., Matsuura, M., & Zijlstra, A.A. 2003, MNRAS, 341, 1205
- Vassiliadis, E., & Wood, P. 1993, ApJ, 413, 641
- Volk, K. & Kwok, S. 1988, ApJ, 331, 435
- Wallerstein, G. & Knapp, G.R. 1998, ARA & A 36, 369
- Winters, J.M., Dominik, C., & Sedlmayr, E. 1994a, A & A, 288, 255
- Winters, J.M., Fleischer, A.J., Gauger, A., & Sedlmayr, E. 1994b, A & A, 290, 623
- Winters, J.M., Fleischer, A.J., Gauger, A., & Sedlmayr, E. 1995, A & A, 302, 483
- Winters, J.M., Lebertre, T., Jeong, K.S., Nyman, L.-A., & Epchtein, N. 2003, A & A, 409, 715
- Wong, T., Schoier, F.L., Lindqvist, M., & Olofsson, H. 2004, A & A, 413, 241